



Fe-doped ZnO nanoparticles: Synthesis by a modified sol-gel method and characterization



Mariani A. Ciciliati ^{a,*}, Marcela F. Silva ^a, Daniela M. Fernandes ^a, Mauricio A.C. de Melo ^b, Ana Adelina W. Hechenleitner ^a, Edgardo A.G. Pineda ^a

^a Departamento de Química, Universidade Estadual de Maringá, Av. Colombo 5790, 87020-900, Zona Sete, Maringá, Brazil

^b Departamento de Física, Universidade Estadual de Maringá, Av. Colombo 5790, 87020-900, Zona Sete, Maringá, Brazil

ARTICLE INFO

Article history:

Received 26 March 2015

Received in revised form

3 June 2015

Accepted 7 June 2015

Available online 18 June 2015

Keywords:

Nanocrystalline materials

Sol-gel preparation

Zinc oxide

ABSTRACT

In this work, Fe-doped and mixed ZnO nanoparticles were synthesized via a modified sol-gel method using water as unique solvent. The structural properties were analyzed by X-ray diffraction and the results showed the existence of wurtzite ZnO structure. The XRD results also indicate a phase segregation in the samples with more than 2 mol% of Fe. UV-Vis diffuse reflectance spectra showed that Fe-doped ZnO exhibited a red-shift of the band-edge and a decrease in band gap energy, as compared to pure ZnO. The surface area increased significantly with the iron addition, and TEM analysis revealed hexagonal nanoparticles.

© 2015 Elsevier B.V. All rights reserved.

1. Introduction

Currently, semiconductor nanostructures have attracted great attention due to their unique physical and chemical properties [1]. ZnO is a n-type semiconductor, with a wide band gap energy (E_g 3.37 eV), and a large exciton binding energy, 60 meV. It has important properties such as chemical and thermal stability, low cost and environmentally safe [2]. ZnO also have excellent optical and electronic properties, which have many applications in photocatalysis, solar cells, gas sensors, and even in sunscreens [3–6].

Transition metal ions such as Cu^{2+} , Co^{2+} , and Fe^{3+} have been used as dopants for ZnO, with the objective of modifying some of their properties [7]. In particular, iron has been investigated in order to improve electrical, optical and magnetic properties. Studies have reported the influence of iron doping in the structure of ZnO, revealing significant improvements in results with the metal addition, in applications such as photocatalysis and gas sensors [8,9].

It is well known that the properties of nanoparticles are sensitive to the conditions of their preparation. ZnO has been prepared by a variety of techniques such as hydrothermal method [10], combustion [11], co-precipitation [12], and sol-gel method [13]. Among these, a modified sol-gel method [14] shows some advantages over the other methods such as being simple, cost

effective and uses only water as solvent. This method was used in this work for ZnO and Fe doped ZnO synthesis. Their structural, morphological and optical properties were characterized by XRD, TEM, diffused reflectance spectroscopy and surface area determination.

2. Material and methods

Aqueous diluted PVA (10% w/v) and saturated metal nitrate solutions ($\text{Zn}(\text{NO}_3)_2 \cdot 6\text{H}_2\text{O}$ and $(\text{Fe}(\text{NO}_3)_3 \cdot 9\text{H}_2\text{O}$) were prepared separately and then mixed at certain metal:monomer unit ratios. The main function of the polymer in the reaction is to provide a polymeric network to hinder cations mobility, allowing local stoichiometry to be maintained and minimizing precipitation of unwanted phases [15].

The solution was maintained at room temperature under stirring for 2 h and then heated to 300 °C under stirring until total water evaporation and partial thermal degradation of the polymer. This product was named as precursor powder. The nanostructured materials were obtained after calcination of the precursor powders under air atmosphere at 400 °C. In this way, Fe-doped ZnO nanoparticles containing different concentrations of Fe^{3+} ions (1, 2, 5, 7, 9 and 10 mol%) were prepared. These samples were called Zn100 (ZnO) and $\text{Fe}(X)\text{Zn}(100-X)$ (doped with X mol% of Fe^{3+} ions).

The crystalline phases were identified by XRD using a Shimadzu XRD-7000 X-ray diffractometer with Cu radiation.

* Correspondence to: Chemistry Department, Universidade Estadual de Maringá, Av. Colombo, 5790, Jardim Universitário, CEP 87020-900 Maringá, Paraná, Brazil.
E-mail address: marianiciciliati@gmail.com (M.A. Ciciliati).

UV-visible diffuse reflectance spectra of the samples were measured with a Perkin-Elmer Lambda 1050 spectrophotometer using integrating sphere attachments. The specific surface area of the particles was evaluated by the N_2 adsorption, using a Quanta Chrome Nova 1000 series, based on the BET method. The morphology of Fe doped ZnO nanopowders was analyzed by transmission electron microscopy using a JEM-1400 JEOL (TEM) instrument.

3. Results and discussion

Fig. 1(a) shows the XRD pattern of the ZnO and Fe-ZnO nanoparticles. All the diffraction peaks are indexed to hexagonal phase ZnO of wurtzite structure (JCPDS 36-1451) [16]. A baseline shift is observed in the 34–36° interval for the samples containing ≥ 2 mol% of Fe, indicating overlapping of peaks. On the other hand, for the Fe10Zn90 sample also emerges a peak at 30°. Peaks at $2\theta=30^\circ$ and 35° , are characteristic of maghemite phase of Fe_2O_3 [15] and can explain the observed behavior. **Fig. 1(b)** shows a magnification of the peak at 36.3° in Zn100 were a shift to lower angle occurs specially in the Fe1Zn99 sample. This result suggests a change in lattice parameters and cell volumes in the hexagonal structure of ZnO [9], confirming that Fe^{3+} is replacing Zn^{2+} in the crystal structure of ZnO.

The average crystallite size (d) was calculated for all samples by Debye-Scherrer's equation,

$$d = \frac{0.9\lambda}{(B \cos \theta_B)} \quad (1)$$

where λ is the wavelength, B the full width at half maximum of the peak (FWHM), and θ_B the Bragg angle. The results are shown in **Table 1**. It is observed that d decreases (from 25 nm to 11 nm) with the increase of Fe concentration until 9 mol%. This probably occurs due to the difference in ionic radius between the metals (approximately 0.68 Å for Fe^{3+} and 0.74 Å for Zn^{2+}) [17] which causes a distortion in the crystal lattice, resulting in greater tension and consequently affecting the crystals growth.

Fig. 2 shows representative TEM images taken from pure ZnO (**Fig. 2a**) and Fe7Zn93 (**Fig. 2b**). In general, all samples show similar morphologies. The images of the ZnO sample revealed that it presents tendency to hexagonal morphology, but Fe7Zn93 sample does not have a definite shape. It is clear that iron addition changes the morphology of the particles.

Table 1

Average crystallite size (d), band gap energy (E_g) and surface area (A) of nanostuctured oxides.

Sample	d (nm)	E_g (eV)	A ($m^2 g^{-1}$), $\sigma=1.12$
ZnO	25	3.1	18.0
Fe1Zn99	19	3.0	26.7
Fe2Zn98	15	2.9	37.5
Fe5Zn95	13	2.8	55.8
Fe7Zn93	12	2.7	49.4
Fe9Zn91	11	2.6	45.6
Fe10Zn90	16	2.3	52.1

The diffuse reflectance spectra are presented in **Fig. 3**. A redshift of the band gap with the incorporation of Fe into ZnO has been observed and interpreted as mainly due to the $sp-d$ exchange interactions between the band electrons and the localized d electrons of the Fe^{3+} ions substituting Zn^{2+} ions [18].

The diffuse reflectance spectra were analyzed by Kubelka-Munk equation:

$$F(R) = \frac{(1-R)^2}{2R} \quad (2)$$

where R is the absolute reflectance of the sampled and $F(R)$ is Kubelka-Munk function [19]. The optical band gap energy E_g of the samples were determined using Tauc's relation:

$$(hv\alpha)^{1/n} = A(\alpha v - E_g) \quad (3)$$

which can be rewritten as for the diffused reflectance calculations:

$$(hvF(R))^{1/n} = A(hv - E_g) \quad (4)$$

where h is the Planck's constant, v the photon frequency, A is an energy-independent constant, n is 1/2 for direct semiconductors and E_g is the optical band gap [20]. The optical band gap of the samples was determined from the plots of $(hvF(R))^2$ versus hv (**Fig. 3** inset). An extrapolation of the linear region of the graph to the energy axis when $(hv)^2 = 0$ gives the band gap values (**Table 1**). It can be observed that the pure ZnO band gap is 3.1 eV, and with the increase in iron doping concentrations until 10 mol%, the band gap decreases. This can be explained considering that with the incorporation of transition metal ions in the crystal lattice of ZnO, more energy levels are added, which creates more defects [21]. Furthermore, the specific surface area of the ZnO is about $18.0 m^2 g^{-1}$ (**Table 1**) and increase in iron dopant content causes

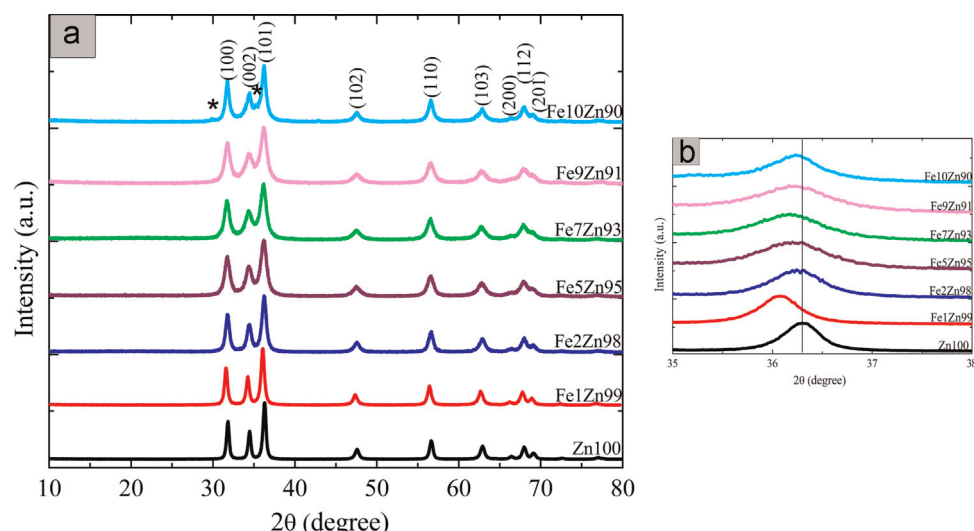


Fig. 1. XRD patterns of the synthesized zinc oxide and Fe doped zinc oxide.

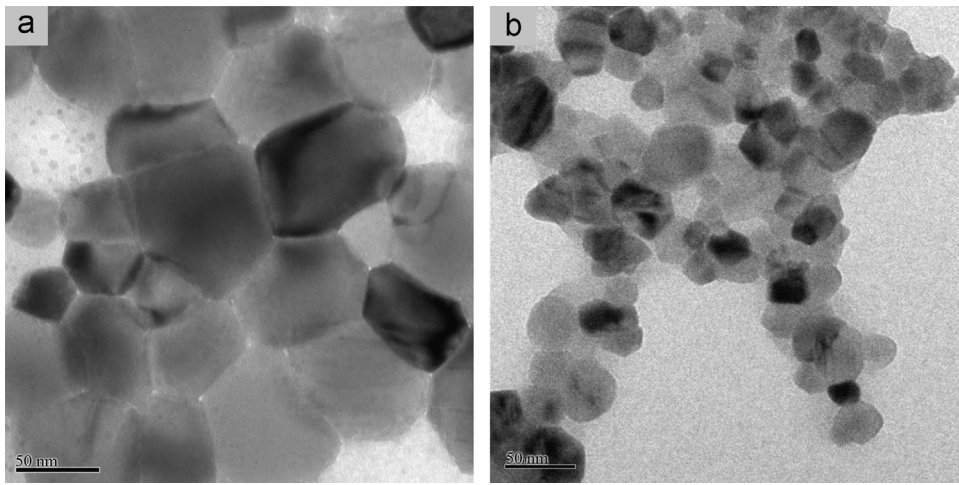


Fig. 2. TEM images of (a) Zn100 and (b) Fe7Zn93 nanoparticles.

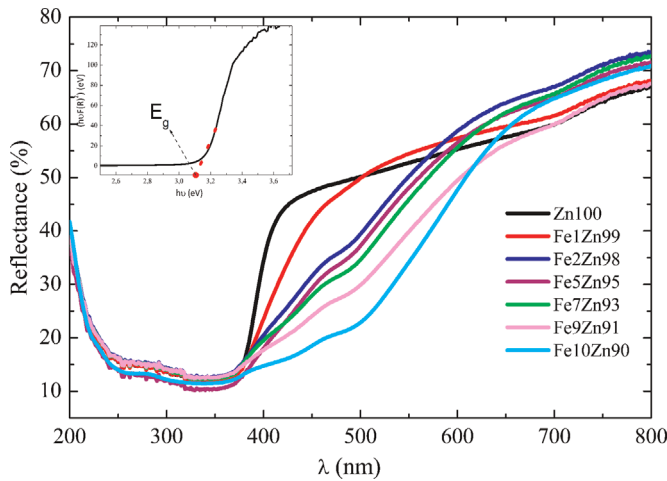


Fig. 3. Diffuse reflectance versus wavelength of nanostructured oxides.

an increase in the surface area, reaching $55.8 \text{ m}^2 \text{ g}^{-1}$ in the Fe5Zn95 sample. This is due to the decrease in crystallite size of the nanoparticles.

4. Conclusion

It was possible to synthesize nanostructured zinc oxide and iron doped zinc oxide by a simple modified sol-gel method. The ZnO could be doped with 1 mol% of Fe ions. Results indicate that, most probably, with more than 2 mol% of Fe, a Fe_2O_3 phase segregation occurs. The average crystallite size of the samples decreased with an increase in the Fe doping amount. The nanoparticles showed a near hexagonal shape. A decrease in the band gap energy was observed from 3.1 eV (ZnO) to 2.3 eV (Fe10Zn90), and the surface area increased from 18 (Zn100) to $55 \text{ m}^2 \text{ g}^{-1}$ (Fe5Zn95).

Acknowledgments

To Universidade Estadual de Maringá (UEM), COMCAP/UEM for all equipments used in this work and CAPES.

References

- [1] M. Lima, D. Fernandes, M. Silva, M. Baesso, A. Neto, G. de Morais, et al., Co-doped ZnO nanoparticles synthesized by an adapted sol-gel method: effects on the structural, optical, photocatalytic and antibacterial properties, *J. Sol-Gel Sci. Technol.* 72 (2014) 301–309.
- [2] A. Srivastava, N. Kumar, S. Khare, Enhancement in UV emission and band gap by Fe doping in ZnO thin films, *Opto-Electron. Rev.* 22 (2014) 68–76.
- [3] R. Murugan, T. Woods, P. Fleming, D. Sullivan, S. Ramakrishna, P. RB, Synthesis and photocatalytic application of ZnO nanoarrows, *Mater. Lett.* 128 (2014) 404–407.
- [4] Q.F. Zhang, C.S. Dandeneau, X.Y. Zhou, G.Z. Cao, ZnO nanostructures for dye-sensitized solar cells, *Adv. Mater.* 21 (2009) 4087–4108.
- [5] J.J. Qi, H. Zhang, S.N. Lu, X. Li, M.X. Xu, Y. Zhang, High performance indium-doped ZnO gas sensor, *J. Nanomater.* (2015) 6.
- [6] S. He, X. Zou, Z. Sun, G. Teng, Influence of precursor solution's concentration on double-layer ZnO structure and solar cell's performance, *Mater. Lett.* 91 (2013) 258–260.
- [7] Z.W. Jin, T. Fukumura, M. Kawasaki, K. Ando, H. Saito, T. Sekiguchi, et al., High throughput fabrication of transition-metal-doped epitaxial ZnO thin films: a series of oxide-diluted magnetic semiconductors and their properties, *Appl. Phys. Lett.* 78 (2001) 3824–3826.
- [8] M.M. Ba-Abbad, A.A.H. Kadhum, A. Mohamad, M.S. Takriff, K. Sopian, Visible light photocatalytic activity of Fe^{3+} -doped ZnO nanoparticle prepared via sol-gel technique, *Chemosphere*, 91 (2013) 1604–1611.
- [9] S. Bai, T. Guo, Y. Zhao, Sun J, D. Li, A. Chen, et al., Sensing performance and mechanism of Fe-doped ZnO microflowers, *Sens. Actuators B: Chem.* 195 (2014) 657–666.
- [10] A. Moulahi, F. Sediri, ZnO nanoswords and nanopills: Hydrothermal synthesis, characterization and optical properties, *Ceram. Int.* 40 (2014) 943–950.
- [11] N.L. Tarwal, P.R. Jadhav, S.A. Vanalakar, S.S. Kalagi, R.C. Pawar, J.S. Shaikh, et al., Photoluminescence of zinc oxide nanopowder synthesized by a combustion method, *Powder Technol.* 208 (2011) 185–188.
- [12] A. Rahmati, A.B. Sircani, M. Molaei, M. Karimipour, Cu-doped ZnO nanoparticles synthesized by simple co-precipitation route, *Eur. Phys. J. Plus* 129 (2014) 7.
- [13] T. Ivanova, A. Harizanova, T. Koutzarova, B. Vertruyen, Study of ZnO sol-gel films: Effect of annealing, *Mater. Lett.* 64 (2010) 1147–1149.
- [14] D.M. Fernandes, R. Silva, A.A.W. Hechenleitner, E. Radovanovic, M.A.C. Melo, E.A.G. Pineda, Synthesis and characterization of ZnO, CuO and a mixed Zn and Cu oxide, *Mater. Chem. Phys.* 115 (2009) 110–115.
- [15] M.F. Silva, L.A.S. de Oliveira, M.A. Ciciliati, L.T. Silva, B.S. Pereira, A.A.W. Hechenleitner, et al., Nanometric particle size and phase controlled synthesis and characterization of $\gamma\text{-Fe}_2\text{O}_3$ or $(\gamma+\alpha)\text{-Fe}_2\text{O}_3$ by a modified sol-gel method, *J. Appl. Phys.* (2013) 114.
- [16] A.A. Ashkarran, A. Iraji zad, S.M. Mahdavi, M.M. Ahadian, ZnO nanoparticles prepared by electrical arc discharge method in water, *Mater. Chem. Phys.* 118 (2009) 6–8.
- [17] T. Pandiyarajan, R. Udayabhaskar, B. Karthikeyan, Role of Fe doping on structural and vibrational properties of ZnO nanostructures, *Appl. Phys. A-Mater. Sci. Process.* 107 (2012) 411–419.
- [18] A.P. Rambu, V. Nica, M. Dobromir, Influence of Fe-doping on the optical and electrical properties of ZnO films, *Superlattices Microstruct.* 59 (2013) 87–96.
- [19] P. Kubelka, New contributions to the optics of intensely light-scattering materials, *J. Opt. Soc. Am.* 38 (1948) 448–457.
- [20] C. Aydin, M.S. Abd El-sadek, K. Zheng, I.S. Yahia, F. Yakuphanoglu, Synthesis, diffused reflectance and electrical properties of nanocrystalline Fe-doped ZnO via sol-gel calcination technique, *Opt. Laser Technol.* 48 (2013) 447–452.
- [21] A. Debernardi, M. Fanciulli, The magnetic interaction of Fe doped ZnO with intrinsic defects: a first principles study, *Phys. B: Condens. Matter* 401–402 (2007) 451–453.